machines

MDPI

Article

Deadbeat Predictive Current Control with High Accuracy Under a Low Sampling Ratio for Permanent Magnet Synchronous Machines in Flywheel Energy Storage Systems

Xinjian Jiang [1,2], Hao Qin [3], Zhenghui Zhao [3], Fuwang Li [1], Zhiru Li [1] and Zhijian Ling [3,*]

[1] Shanxi Energy Internet Research Institute, Taiyuan 030000, China; 15931101616@139.com (F.L.)
[2] Department of Electrical Engineering, Tsinghua University, Beijing 100084, China
[3] School of Electrical and Information-Engineering, Jiangsu University, Zhenjiang 212013, China; zhzhao@ujs.edu.cn (Z.Z.)
* Correspondence: lzj1991@ujs.edu.cn

Abstract

The predictive current control for the permanent magnet synchronous machine (PMSM) shows great potential in applications like flywheel energy storage, owing to its fast dynamic response and simple structure. However, under low carrier ratio conditions, conventional deadbeat predictive current control (DPCC) exhibits drawbacks such as significant current prediction error, inaccurate instruction voltage calculation, and severe torque and flux linkage coupling. This paper proposes an improved DPCC method suitable for both high and low carrier ratio operation of the PMSM. First, a modified stator voltage equation is established considering rotor flux orientation error. By treating the *dq*-coordinates as stationary and accounting for rotor rotation within the control period, a dynamic PMSM model is developed, effectively suppressing cross-axis coupling under low carrier ratios. Simultaneously, a multi-coordinate variable synchronization method is also introduced to eliminate prediction and voltage errors caused by cross-coordinate computation, enabling precise deadbeat control across all carrier ratios. The experimental results demonstrate that the proposed method enhances torque-flux decoupling, improves current prediction and tracking accuracy at low carrier ratios, and offers a reliable solution for dynamic control in flywheel energy storage systems.

Keywords: coordinate system synchronization; current prediction; low carrier ratio; modified voltage equation; permanent magnet synchronous machine

check for updates

Academic Editor: Payam Shams Ghahfarokhi

Received: 26 September 2025
Revised: 11 October 2025
Accepted: 27 October 2025
Published: 29 October 2025

Citation: Jiang, X.; Qin, H.; Zhao, Z.; Li, F.; Li, Z.; Ling, Z. Deadbeat Predictive Current Control with High Accuracy Under a Low Sampling Ratio for Permanent Magnet Synchronous Machines in Flywheel Energy Storage Systems. *Machines* **2025**, *13*, 995. https://doi.org/10.3390/machines13110995

Copyright: © 2025 by the authors. Licensee MDPI, Basel, Switzerland. This article is an open access article distributed under the terms and conditions of the Creative Commons Attribution (CC BY) license (https://creativecommons.org/licenses/by/4.0/).

1. Introduction

Flywheel energy storage systems, as an efficient and reliable kinetic energy storage technology [1,2], impose stringent requirements on drive machines, including high power density, wide speed range, fast torque response, and low-loss operation. The PMSM, with its high power density, high reliability, and excellent dynamic performance [3,4], has become an ideal choice for flywheel energy storage applications. Its control performance directly affects the energy conversion efficiency and operational stability of the entire system. As the demands for higher power and speed in aerospace, electric vehicles, and industrial equipment, drive systems face greater challenges. Conventional vector control based on PI regulators suffers from difficulties in parameter tuning and balancing dynamic and steady-state performance under high-speed and high-power conditions. In contrast, DPCC, which utilizes a machine model for feedforward prediction, offers advantages such

as fast dynamic response and elimination of parameter tuning, making it more suitable for high-performance applications like flywheel energy storage.

In low-speed high-power and high-speed applications, the carrier ratio—defined as the ratio of the inverter switching frequency to the fundamental frequency of the machine—is often limited due to switching losses, thermal constraints, and system efficiency. A carrier ratio below 15 is typically considered low. Under such conditions, the model error of conventional DPCC increases significantly [5,6]. On the one hand, discretization errors and control delays have a more pronounced impact on control accuracy and system stability; on the other hand, the larger electrical angle increment within a single control cycle exacerbates the coupling between torque and flux. Excessively low carrier ratios may even lead to current loop instability [7,8].

To address these issues, existing research on low-carrier-ratio machine control has focused mainly on delay compensation, discrete errors, and rotor movement effects [9]. First, discrete control introduces a zero-order hold effect with a delay of 1 T_s, which reduces control bandwidth and can destabilize dynamic processes. A common compensation method is to add phase lead [10,11]; some studies also account for the 0.5 T_s pulse width modulation (PWM) delay [12], though such approaches often overlook the timeliness of the voltage reference. Second, the discrete nature of the controller also leads to current sampling errors. The *dq*-axis currents calculated from sampled values at the current instant may not accurately represent the actual values over the entire control period. In [13], an open-loop model-based error estimator to compensate for discrete current sampling errors was proposed. Furthermore, discretizing the continuously rotating rotor reference frame inevitably introduces rotor movement effects, causing deviations between the output voltage and reference voltage—especially non-negligible at low carrier ratios. To counteract voltage reference errors due to rotor movement, the average reference voltage based on volt-second equivalence is applied [12], combined with delay compensation, to match output and reference voltages. Synchronous transformation is avoided via deadbeat control using flux linkage in the stationary frame, albeit at the cost of higher computational burden [13]. For torque and flux coupling, complex vector decoupling models with zero-pole cancelation are adopted [14–17] to reduce dq-axis coupling. This method, however, suffers from limited bandwidth and inadequate dynamic performance. Meanwhile, in [18] it is demonstrated that the controller zeros designed for a continuous system cannot accurately cancel the poles of the discrete motor model, with the cancelation precision degrading as the carrier ratio decreases. In [19], an online least squares support vector machine is utilized to construct an inverse system for the PMSM, achieving system linearization and decoupled control; however, this method depends critically on the accuracy and response speed of the flux observer. Furthermore, overcurrent risks and multi-source disturbances also pose critical challenges to high-performance PMSM control. To address these issues, studies have employed methods such as current-constrained sliding mode control to enhance system robustness [20,21]. However, these approaches primarily focus on anti-disturbance design for single-loop speed control systems and do not resolve the inherent model inaccuracies and multi-coordinate computational discrepancies in deadbeat predictive current control under low carrier ratio conditions.

The above analysis indicates that as the carrier ratio decreases, control methods based on conventional rotor reference frame models exhibit increasingly prominent limitations. Most existing studies focus on compensation strategies rather than addressing inherent model inaccuracies. In fact, under low carrier ratios, the conventional stator voltage equation in the synchronous rotating frame is no longer applicable, leading to inherent model errors in conventional DPCC. Moreover, the participation of variables from multiple coordinate systems in the prediction process introduces additional computational errors.

Therefore, this paper establishes a modified stator voltage equation that accounts for rotor flux orientation error, thereby mitigating *dq*-axis coupling under low carrier ratios. Furthermore, a multi-coordinate variable synchronization method is proposed to eliminate prediction and voltage reference errors caused by cross-frame calculations, achieving accurate deadbeat predictive current control suitable for both high and low carrier ratio operation of PMSMs.

2. Conventional Non-Sampled Predictive Current Control

2.1. Control Principle

The implementation of conventional DPCC primarily involves current prediction and reference voltage calculation [22–24]. First, the sampled values of the stator currents are substituted into the discrete machine voltage equation to predict the current for the next control cycle. A one-step delay compensation is applied to counteract the inherent one-control-step delay of the digital controller. Subsequently, the reference current values and the predicted current values are substituted into the discrete machine voltage equation to calculate the reference voltage for the next control cycle. The control objective is to force the actual current at the end of the control cycle to equal its reference value, thereby realizing deadbeat predictive current control. A system block diagram of the conventional DPCC strategy is shown in Figure 1.

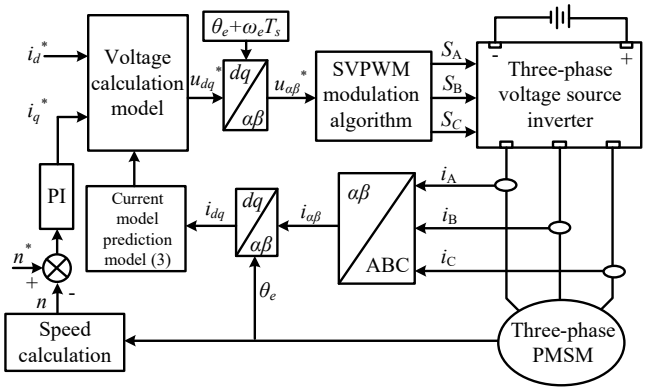


Figure 1. System block diagram of PMSM DPCC strategy.

In the rotor synchronous rotating reference coordinate, the stator voltage equations of a PMSM are shown as follow:

$$\begin{cases} u_d = R_s i_d + L_d \frac{di_d}{dt} - \omega_e L_q i_q \\ u_q = R_s i_q + L_q \frac{di_q}{dt} + \omega_e (L_d i_d + \psi_f) \end{cases} \tag{1}$$

where u_d, u_q, and i_d, i_q are the *d*-axis and *q*-axis components of the stator voltage and current, respectively; R_s is the stator phase resistance; L_d and L_q are the *d*-axis and *q*-axis inductances, respectively; ψ_f is the PM flux linkage; and ω_e is the electrical angular velocity.

By discretizing Equation (1) using the forward Euler method, the discrete equation for the stator voltage of the machine can be obtained:

$$\begin{cases} {u_d}^{k+1} = R_s {i_d}^{k+1} + \frac{L_d}{T_s}(i_d^{*k+2} - {i_d}^{k+1}) - \omega_e L_q {i_q}^{k+1} \\ {u_q}^{k+1} = R_s {i_q}^{k+1} + \frac{L_q}{T_s}(i_q^{*k+2} - {i_q}^{k+1}) + \omega_e (L_d {i_d}^{k+1} + \psi_f) \end{cases} \tag{2}$$

where u_d^{k+1}, u_q^{k+1}, i_d^{k+1}, i_q^{k+1} are, respectively, the command voltage *d* and *q*-axis components and the predicted current value *d* and *q*-axis components at $(k+1)T_s$ moment; i_d^{*k+2} and i_{*k+2} are, respectively, the *d* and *q*-axis current components of the given current at $(k+2)T_s$. T_s represents the control period.

Rewriting Equation (2) provides the discrete model with one-step delay compensation for the current, the calculation formula for the predicted current, as shown in Equation (3).

$$\begin{cases} {i_d}^{k+1} = (1 - \frac{T_s R_s}{L_d}){i_d}^k + \frac{T_s}{L_d}{u_d}^k + \frac{T_s \omega_e}{L_d} L_q {i_q}^k \\ {i_q}^{k+1} = (1 - \frac{T_s R_s}{L_q}){i_q}^k + \frac{T_s}{L_q}{u_q}^k - \frac{T_s \omega_e}{L_q}(L_d {i_d}^k + \psi_f) \end{cases} \tag{3}$$

where i_d^k and i_q^k are, respectively, the d-axis and q-axis components of the stator current sampling value at the kT_s moment.

To eliminate the controller output delay, compensation for the delayed output angle of the reference voltage is also required. This is because the calculated d-axis and q-axis voltages at the current instant will be output at the next instant. Therefore, when transforming the d-axis and q-axis reference voltages to the α-β plane via the Park transformation, the predicted rotor position angle for the $k + 1$ instant should be used. Since the mechanical time constant is much larger than the electrical time constant, the electrical angular velocity ω_e can be assumed constant over one control period. The estimated rotor position for the next cycle can be expressed as $\theta_e + \omega_e T_s$. Thus, the calculation of the reference voltage in the α-β plane is:

$$\begin{bmatrix} u_\alpha^* \\ u_\beta^* \end{bmatrix} = \begin{bmatrix} \cos(\theta_k + \omega_e T_s) & -\sin(\theta_k + \omega_e T_s) \\ \sin(\theta_k + \omega_e T_s) & \cos(\theta_k + \omega_e T_s) \end{bmatrix} \begin{bmatrix} {u_d}^{k+1} \\ {u_q}^{k+1} \end{bmatrix} \tag{4}$$

Deadbeat predictive current control can be accomplished based on Equations (2)–(4). It is important to note that the accuracy of the conventional deadbeat control model relies on the assumption that the d-axis remains perfectly aligned with the rotor flux linkage. However, this premise does not hold in discrete control systems, particularly under low carrier ratio conditions. Violation of this assumption leads to significant model errors.

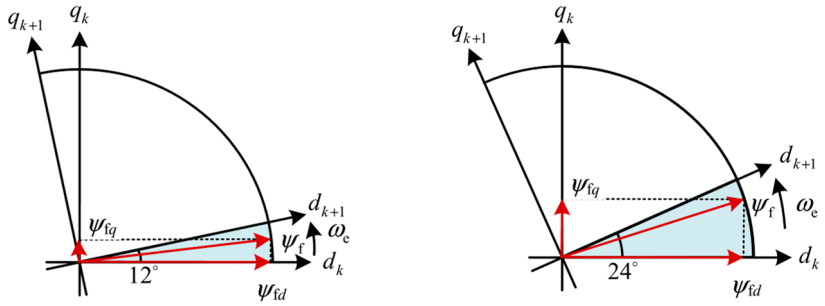
2.2. Analysis of Control Errors

The primary sources of error in conventional deadbeat predictive current control are machine model inaccuracies caused by discrete control and rotor rotation effects, and calculations involving variables from multiple coordinate systems across different mathematical spaces.

When establishing the stator voltage equation using the conventional method, it is assumed that the d-axis is always aligned with the rotor flux linkage, meaning the dq-coordinate system rotates continuously with the rotor. In reality, within a discrete control system, the position of the d-axis remains fixed at the sampled rotor position value throughout a single control period, effectively making it stationary. Meanwhile, the rotor continues to rotate continuously. Although their directions coincide at the beginning of the cycle, the rotor flux linkage begins to lead the d-axis over time, and this lead angle gradually increases, resulting in a growing rotor field orientation error. Consequently, the conventional assumption of perfect alignment is invalid in discrete control. Therefore, the machine model derived from the conventional method, while accurate and error-free in the continuous domain, exhibits inherent model errors in discrete control. As the carrier ratio decreases, the rotor orientation error increases, exacerbating this model error. This intensifies the coupling between the stator current's excitation and torque components, leading to control inaccuracies and potentially even system instability under severe conditions.

The rotor orientation error within a single control period caused by the rotor rotation effect under carrier ratios of 30 and 15 are shown in Figure 2, respectively. As shown in Figure 2, when the carrier ratio is 30, the phase difference between the d-axis and the rotor flux linkage at the end of the control period is $360^\circ/30 = 12^\circ$, resulting in a small

component of the PM flux linkage on the q-axis. When the carrier ratio is 15, the phase difference increases to 360°/15 = 24°, this leads to a significantly larger component of the PM flux linkage on the q-axis. This indicates that at lower carrier ratios, the rotor rotation effect aggravates the coupling between the machine's excitation and torque components. Employing conventional deadbeat predictive current control under these conditions will inevitably lead to substantial prediction and control errors, adversely affecting the dynamic and static performance of the machine, and potentially causing system instability.



(**a**) The carrier ratio is 30 (**b**) The carrier ratio is 15

Figure 2. Rotor field orientation error under different carrier ratios.

Furthermore, due to the rotor rotation, the spatial position of the synchronous rotating coordinate system differs at each instant, meaning each moment corresponds to a distinct mathematical space. In the prediction process, the reference coordinate system for the sampled current values is the dq-coordinate at time k, the reference coordinate for the predicted current is the dq-coordinate at time $k + 1$, and the reference coordinate for the current commands is the dq-coordinate at time $k + 2$. Directly using variables from these three different coordinate systems in calculations across mathematical spaces inevitably introduces errors in both current prediction and reference voltage calculation.

The simulation results using conventional deadbeat control under a carrier ratio of 15 (370 r/min, control frequency 2 kHz) are shown in Figure 3. The simulation parameters are listed in Table 1. The results demonstrate that as the speed increases and the carrier ratio decreases, the d-axis and q-axis currents gradually deviate from their reference values, and the speed cannot track its reference, exhibiting a steady-state error.

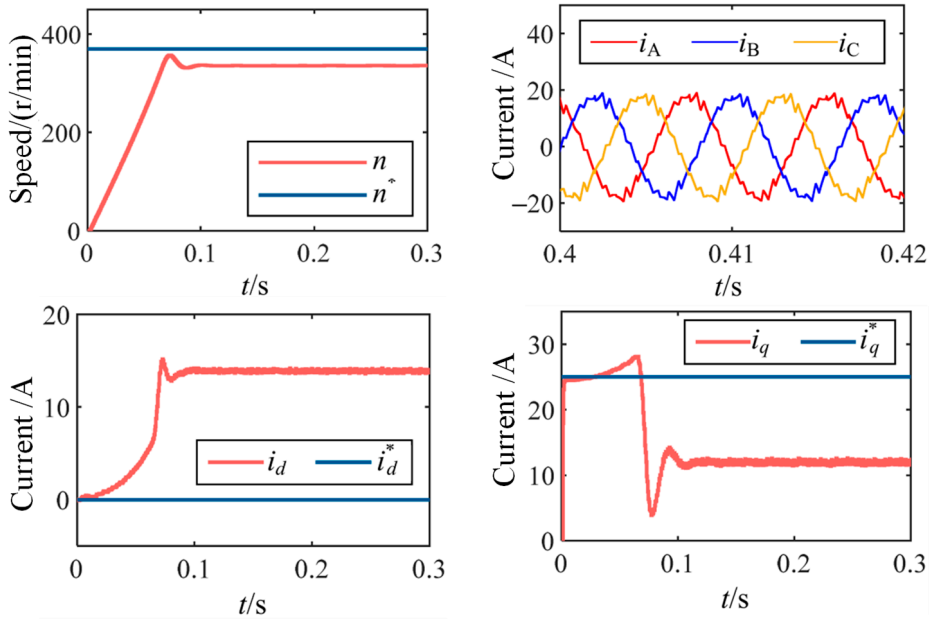


Figure 3. Simulation results of conventional DPCC under low carrier ratio.

Table 1. Parameters of controller and PMSM.

Items	Value
Rated speed $n_N/(r/min)$	370
Rated voltage U_N/V	400
Rated current I_N/A	17
Number of pole-pairs	22
Phase resistance R_S/Ω	0.54
d-axis inductance L_d/mH	5.8
q-axis inductance L_q/mH	6.9
PM flux linkage ψ_f/Wb	0.18
Rotor moment of inertia $J/(kg{\cdot}m^2)$	0.1
Dead time T_d/us	3

3. Low Carrier Ratio Deadbeat Predictive Current Control

3.1. Stator Voltage Equation Considering Rotor Field Orientation Error

The proposed method fundamentally differs from existing flux-oriented approaches by reconceptualizing the reference frame foundation. Rather than applying compensatory corrections to conventional models, we establish a modified stator voltage equation that treats the dq-coordinates as stationary within each control period—a paradigm shift that more accurately represents the physical reality of discrete control systems. This core innovation, combined with explicit incorporation of rotor movement through volt-second equivalent back-EMF calculation, addresses the inherent model inaccuracies that compensatory techniques cannot fully resolve.

Since the dq-coordinate system is stationary within a single control period, there is no mutual cutting between the d and q-axis stator flux linkages, allowing the removal of the back-EMF cross-coupling terms present in conventional dq-coordinate voltage equations. Meanwhile, due to the relative motion between the rotor and the d-axis, the back-EMF generated by the moving PM flux linkage in the stationary dq-coordinate system must be considered. Based on the above analysis, the modified voltage and flux linkage equations for the PMSM are given in Equation (5).

$$\begin{cases} u_d = R_s i_d + \frac{d\psi_d}{dt} \\ u_q = R_s i_q + \frac{d\psi_q}{dt} \\ \psi_d = L_d i_d + \psi_f \cos[\omega_e(t - kT_s)] \\ \psi_q = L_q i_q + \psi_f \sin[\omega_e(t - kT_s)] \end{cases} \tag{5}$$

where kTs is the current sampling time, and kTs $\leq t < (k + 1)T$s. The modified Equation (5) can lead to the corrected stator voltage equation:

$$\begin{cases} u_d = R_s i_d + L_d \frac{di_d}{dt} - \omega_e \psi_f \sin[\omega_e(t - kT_s)] \\ u_q = R_s i_q + L_q \frac{di_q}{dt} + \omega_e \psi_f \cos[\omega_e(t - kT_s)] \end{cases} \tag{6}$$

In the modified voltage equations, the back-EMF terms generated by the PM flux linkage, $\omega_e \Psi_f \sin[\omega_e(t - kT_s)]$ and $\omega_e \Psi_f \sin[\omega_e(t - kT_s)]$, vary continuously within a single control period, making direct Euler discretization of Equation (6) infeasible. In machine drive systems, the mechanical time constant is much larger than the control period. Assuming the electrical angular velocity ω_e remains constant during the control period, it can be observed from Equation (6) that the PM flux back-EMF terms depend solely on time t. Therefore, based on the volt-second equivalence principle, the equivalent values of the PM flux back-EMF on the d and q-axis can be calculated using Equation (7).

$$\begin{cases} \frac{1}{T_s}\int_{kT_s}^{(k+1)T_s} \omega_e \psi_f \sin[\omega_e(t-kT_s)]\mathrm{d}t = \frac{\psi_f}{T_s}(1-\cos\omega_e T_s) \\ \frac{1}{T_s}\int_{kT_s}^{(k+1)T_s} \omega_e \psi_f \cos[\omega_e(t-kT_s)]\mathrm{d}t = \frac{\psi_f}{T_s}\sin\omega_e T \end{cases} \tag{7}$$

Replacing the PM flux back-EMF terms in Equation (6) with the expressions on the right-hand side of Equation (7) yields the stator voltage equations that account for rotor field orientation error, as shown in Equation (8).

$$\begin{cases} u_d = R_s i_d + L_d \frac{\mathrm{d}i_d}{\mathrm{d}t} - \frac{\psi_f}{T_s}(1-\cos\omega_e T_s) \\ u_q = R_s i_q + L_q \frac{\mathrm{d}i_q}{\mathrm{d}t} + \frac{\psi_f}{T_s}\sin\omega_e T_s \end{cases} \tag{8}$$

Compared with Equation (1), Equation (8) treats the *dq*-coordinate system as a stationary coordinate, considers the rotational motion of the rotor during the control period, and enables dynamic modeling of the machine. Based on the improved voltage equation, an accurate and deadbeat predictive current control strategy applicable to both high and low carrier ratios is proposed.

3.2. Consider the DPCC Strategy for Multi-Coordinate System Variable Synchronization

By discretization Equation (8) using the forward Euler method and organizing it, a one-step delay compensation model can be obtained, that is, the current prediction value Equation (9).

$$\begin{cases} i_{dp}^k = (1-\frac{T_s R_s}{L_d}) i_d^k + \frac{T_s}{L_d} u_d^k + \frac{\psi_f}{L_d}(1-\cos\omega_e T_s) \\ i_{qp}^k = (1-\frac{T_s R_s}{L_q}) i_q^k + \frac{T_s}{L_q} u_q^k - \frac{\psi_f}{L_q}\sin\omega_e T \end{cases} \tag{9}$$

where x^k is the value of variable in the *dq*-coordinate system at time step *k*, x^{k+1} and x^{k+2} is similar.

For current prediction, the sampled phase currents are first transformed into the *dq*-coordinate system to obtain the sampled current values i_{dq}^k at time *k*. Both i_{dq}^k and the commanded voltage values u_{dq}^k in the *dq*-coordinate system at time *k* are substituted into the prediction model to obtain the predicted current values i_{dqp}^k, in the *dq*-coordinate system at time *k*. However, due to the discrete nature of the controller and changes in rotor position, the *dq*-coordinate system shifts in the next control cycle. To accurately predict the current i_{dqp}^{k+1} at time $k+1$, the predicted current i_{dqp}^k (in the *dq*-coordinate at time *k*) must be synchronized to the *dq*-coordinate system at time $k+1$ via a Park transformation. Failure to do so will introduce a current prediction error Δi_{dqp}, as illustrated in Figure 4. Equation (10) provides the synchronization formula for the predicted current.

$$\begin{bmatrix} i_{dp}^{k+1} \\ i_{qp}^{k+1} \end{bmatrix} = \begin{bmatrix} \cos\omega_e T_s & \sin\omega_e T_s \\ -\sin\omega_e T_s & \cos\omega_e T_s \end{bmatrix} \begin{bmatrix} i_{dp}^k \\ i_{qp}^k \end{bmatrix} \tag{10}$$

Similarly, the output i_{dq}^{*k+2} from the speed outer loop corresponds to the commanded excitation and torque current components at time $k+2$. Owing to controller discretization and rotor movement, directly using these values to compute the commanded voltage would cause coupling between the excitation and torque components. Therefore, the commanded current values in the *dq*-coordinate system at time $k+2$ must be synchronized back to the *dq*-coordinate at time $k+1$ using an inverse Park transformation. Otherwise, a commanded current error Δi_{dq}^* will occur, as shown in Figure 4. Equation (11) gives the synchronization formula for the commanded current.

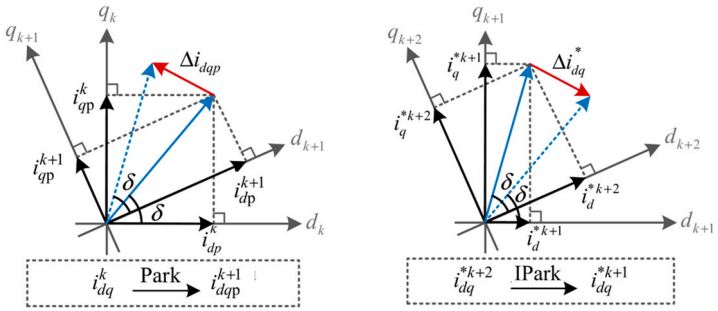


Figure 4. Variables synchronous of multiple *dq* coordinate systems.

$$\begin{bmatrix} i_d^{*k+1} \\ i_q^{*k+1} \end{bmatrix} = \begin{bmatrix} \cos\omega_e T_s & -\sin\omega_e T_s \\ \sin\omega_e T_s & \cos\omega_e T_s \end{bmatrix} \begin{bmatrix} i_d^{*k+2} \\ i_q^{*k+2} \end{bmatrix} \tag{11}$$

By discretizing Equation (8) using the forward Euler method, a new discrete stator voltage equation is obtained. Substituting the synchronized variables across the three coordinate systems at times k, $k+1$, and $k+2$ yields the commanded voltage calculation formula:

$$\begin{cases} u_d^{*k+1} = R_s i_d^{k+1} + \frac{L_d}{T_s}(i_d^{*k+1} - i_d^{k+1}) - \frac{\psi_f}{T_s}(1 - \cos\omega_e T_s) \\ u_q^{*k+1} = R_s i_d^{k+1} + \frac{L_q}{T_s}(i_q^{*k+1} - i_q^{k+1}) + \frac{\psi_f}{T_s}\sin\omega_e T \end{cases} \tag{12}$$

Based on Equations (9)–(12), precise deadbeat predictive current control can be achieved.

Building upon the improved voltage equation and the multi-coordinate variable synchronization method, the proposed deadbeat predictive current control effectively addresses errors caused by rotor flux linkage orientation deviation and cross mathematical space calculations involving variables from multiple coordinate systems. It achieves accurate deadbeat predictive current control suitable for both high and low carrier ratio conditions. The system block diagram of the improved DPCC strategy is shown in Figure 5.

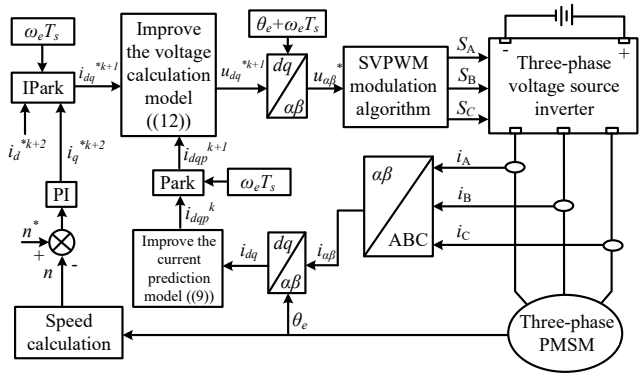


Figure 5. System block diagram of proposed DPCC strategy.

4. Simulated Analysis

A simulation model for PMSM drives was established using the MATLAB/Simulink R2020a platform. The parameters of the target PMSM and the controller are listed in Table 1. The simulation results under improved deadbeat control with a carrier ratio of 15 (370 r/min, control frequency of 2 kHz) are shown in Figure 6.

Compared with Figure 3, it can be observed that the improved method achieves better tracking of the d and q axis current references and exhibits superior dynamic and steady-state performance in the current loop. Meanwhile, the speed remains stable at 370 r/min without steady-state error. This indicates that the deadbeat control strategy based on the improved voltage model and coordinate system synchronization eliminates the model

errors caused by discrete control delay and rotor rotation effects under low carrier ratio conditions, thereby achieving accurate decoupling between d and q axis variables.

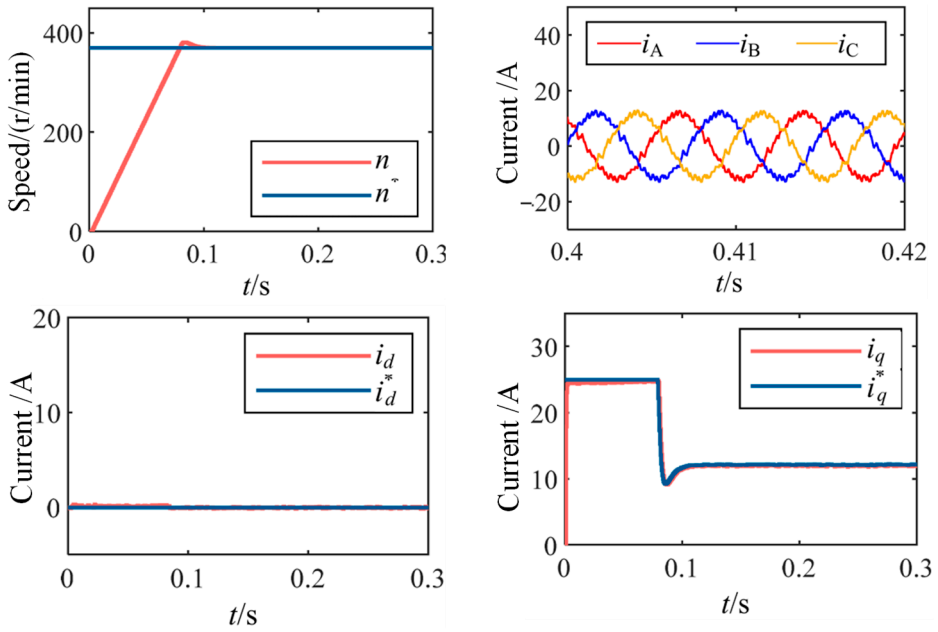


Figure 6. Simulation results of proposed DPCC under low carrier ratio.

A comparison of the d and q axis current prediction errors under two deadbeat predictive current control methods at different carrier ratios is presented in Figure 7. The prediction error is calculated using the following formula (taking the average value over 1 s in steady state).

$$\begin{cases} i_{dqp}^{\mathrm{err}}(z) = i_{dqp}(z) \cdot z^{-1} - i_{dq}^{k}(z), \text{ Conventional method} \\ i_{dqp}^{\mathrm{err}}(z) = i_{dqp}^{k+1}(z) \cdot z^{-1} - i_{dq}^{k}(z), \text{ Improved method} \end{cases} \tag{13}$$

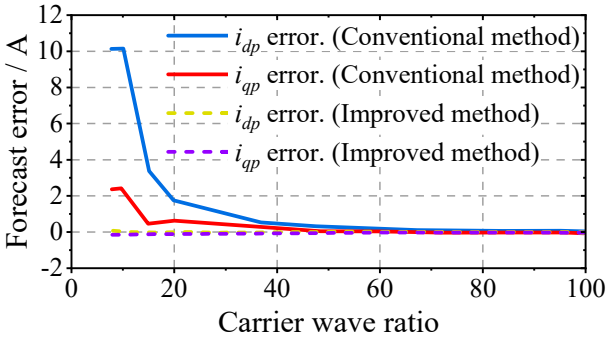


Figure 7. Different DPCC strategies d-q currents prediction error.

When the carrier ratio is above 40, both deadbeat control strategies show similar current prediction accuracy, which remains within an acceptable range. When the carrier ratio is between 15 and 40, the d and q axis current errors of the conventional DPCC strategy gradually increase as the carrier ratio decreases, while the improved DPCC maintains high prediction accuracy. When the carrier ratio falls below 15, the prediction errors of the conventional DPCC increase sharply, making it impossible to maintain stable machine operation. In contrast, the improved DPCC still demonstrates high prediction accuracy and maintains satisfactory control performance.

Furthermore, to verify the performance of the proposed method under high-speed and low carrier ratio conditions, simulations were carried out for such scenarios. The simulation results for a high-speed PMSM with 4 pole pairs operating at 20,000 r/min with

a control frequency of 20 kHz, corresponding to a carrier ratio of 15, are shown in Figure 8. The simulation results are consistent with those under low-speed and low carrier ratio conditions, demonstrating the effectiveness of the proposed method in high-speed and low carrier ratio applications.

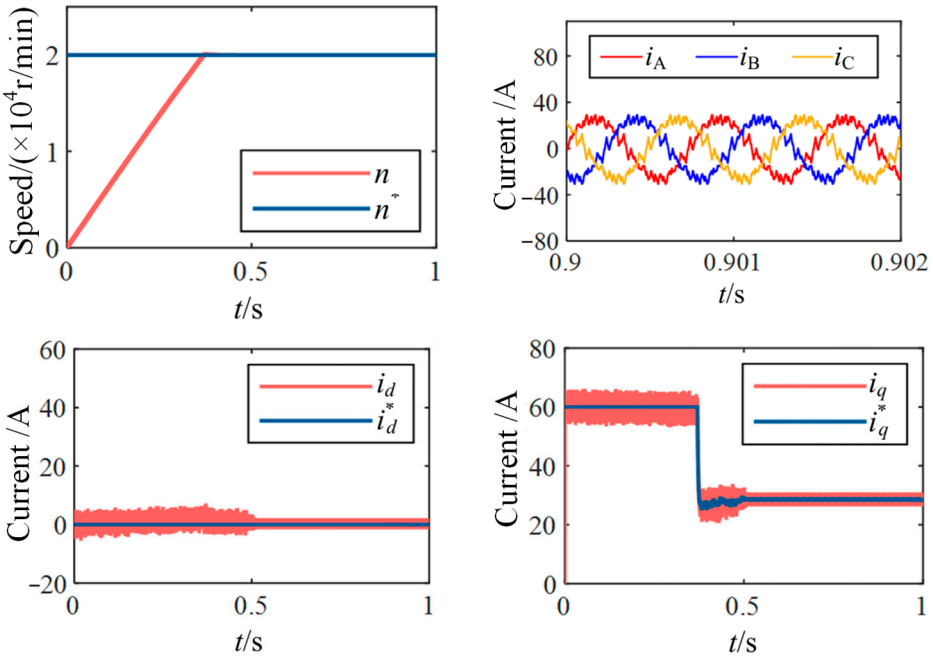


Figure 8. Simulation results of proposed DPCC under high speed and low carrier ratio.

5. Experimental Result

The experimental validation presented in this section not only verifies the effectiveness of the proposed method but also demonstrates its distinct advantages over existing predictive control strategies. Most notably, the maintained stability at carrier ratios as low as 7.4 represents a significant extension of the practical operating range achievable with DPCC, addressing a critical limitation in high-speed drive applications. To validate the feasibility of the theoretical analysis and the effectiveness of the proposed method, an experimental platform was established as shown in Figure 9. The platform mainly consists of a drive unit, a three-phase machine, and a load machine. The core of the drive control unit employs a DSP (TMS320F28377D) plus FPGA architecture. The parameters of the target PMSM are listed in Table 1.

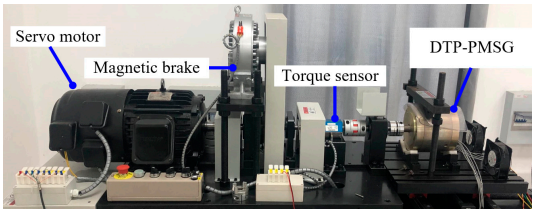


Figure 9. Experimental system.

To verify the effectiveness of the proposed algorithm, steady-state experiments under different carrier ratios were conducted using both conventional and the proposed methods. The machine was maintained at the rated speed of 370 r/min, with control frequencies set to 10 kHz, 2 kHz, and 1 kHz, corresponding to carrier ratios (CR) of 73.7, 14.7, and 7.4, respectively. The comparative waveforms of the d and q axis currents under conventional DPCC and improved DPCC algorithms are shown in Figures 10 and 11, respectively. It can be observed that at higher carrier ratios, both conventional and improved DPCC

exhibit satisfactory tracking performance for the d and q axis currents. As the carrier ratio decreases, the d and q axis currents under the conventional method gradually deviate from the reference values and even oscillate severely, leading to a complete loss of control. In contrast, the proposed method maintains accurate tracking of the reference currents without steady-state error, although the current ripple increases slightly and the pulsation of d and q axis currents slightly amplifies as the carrier ratio decreases.

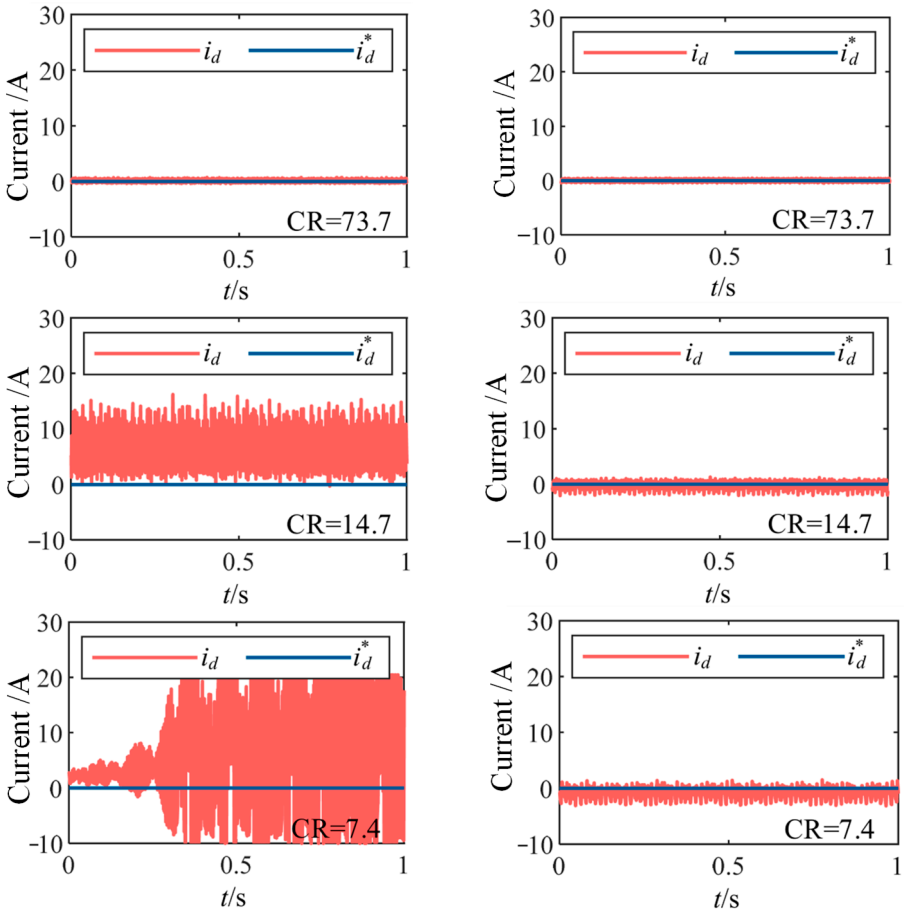
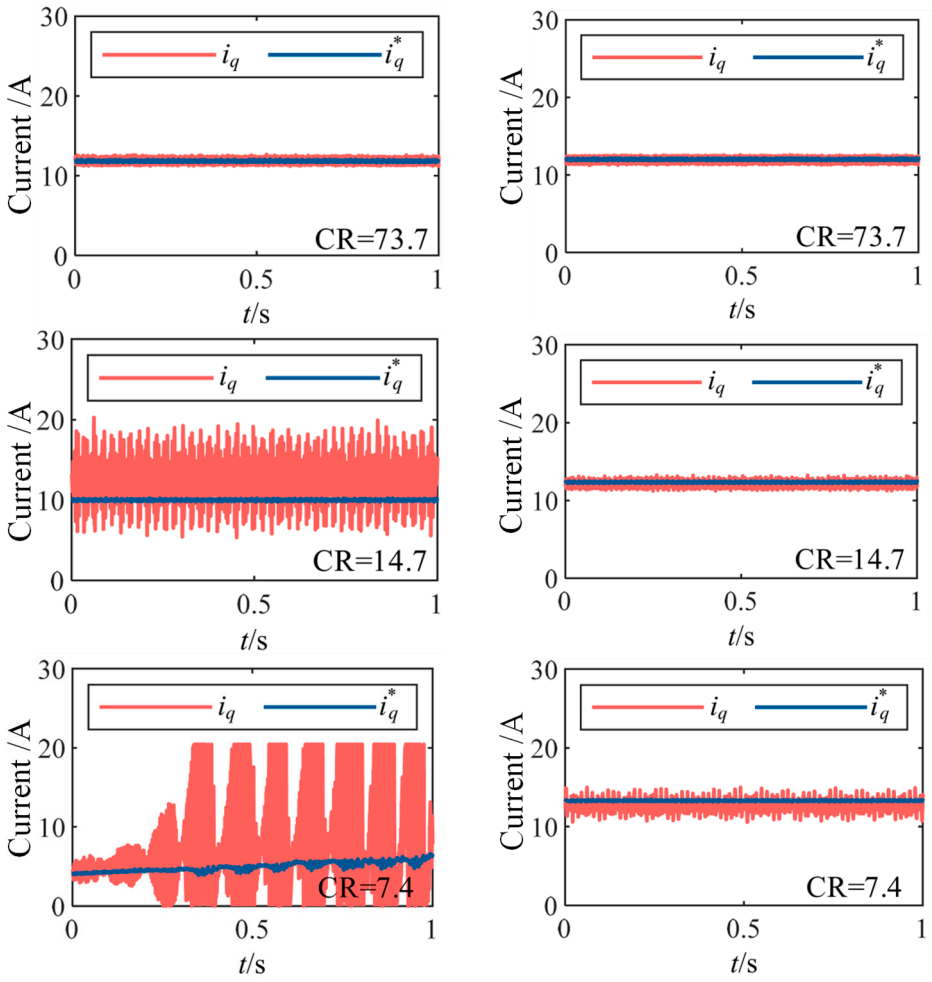


Figure 10. d-axis current wave of both DPCC methods under different carrier ratio.

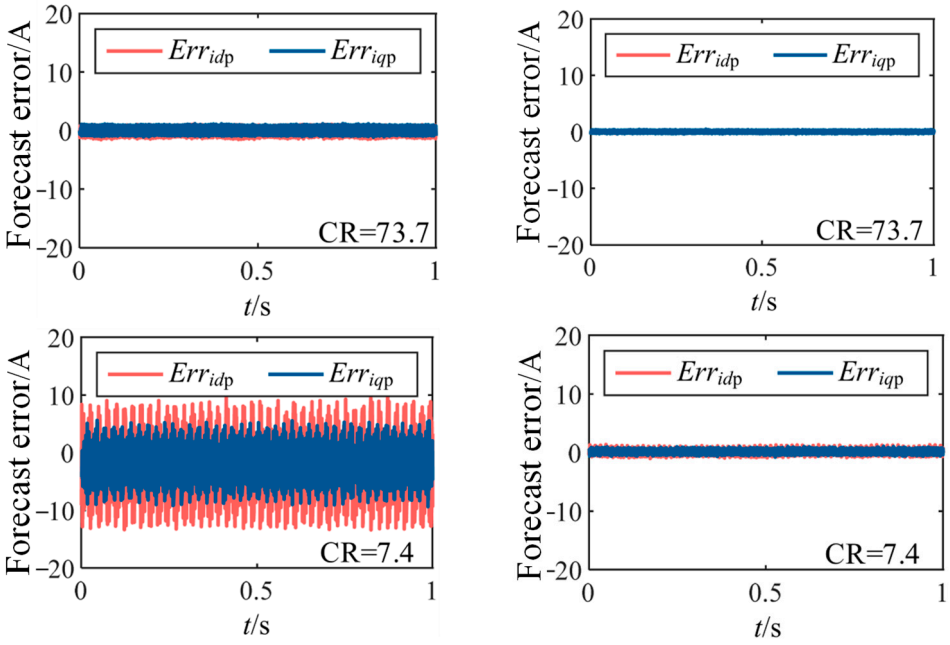
In deadbeat control, both tracking error and prediction error reflect the accuracy of the predictive model. Therefore, based on the tracking error experiments, the prediction errors of the d and q axis currents under the two DPCC strategies were further compared at control frequencies of 10 kHz and 2 kHz. The experimental results are shown in Figure 12. It can be seen that whether at high or low carrier ratios, the proposed method yields smaller prediction errors in the d and q axis currents compared to the conventional method, and the errors remain nearly zero.

To separately verify the effectiveness of the stator voltage equation considering rotor magnetic field orientation error and the multi-coordinate synchronization algorithm in the proposed method, the controller first operated with the conventional DPCC algorithm. After the system reached steady state (t = 2.1 s), the multi-coordinate synchronization algorithm was activated. Then, after 2.5 s (t = 4.6 s), the current prediction model and command voltage calculation model based on the improved stator voltage equation were enabled, constituting the complete proposed method. The experimental results are shown in Figure 13.



(**a**) Conventional method (**b**) Improved method

Figure 11. *q*-axis current wave of both DPCC methods under different carrier ratio.



(**a**) Conventional method (**b**) Improved method

Figure 12. Current prediction errors of both DPCC methods under different carrier ratio.

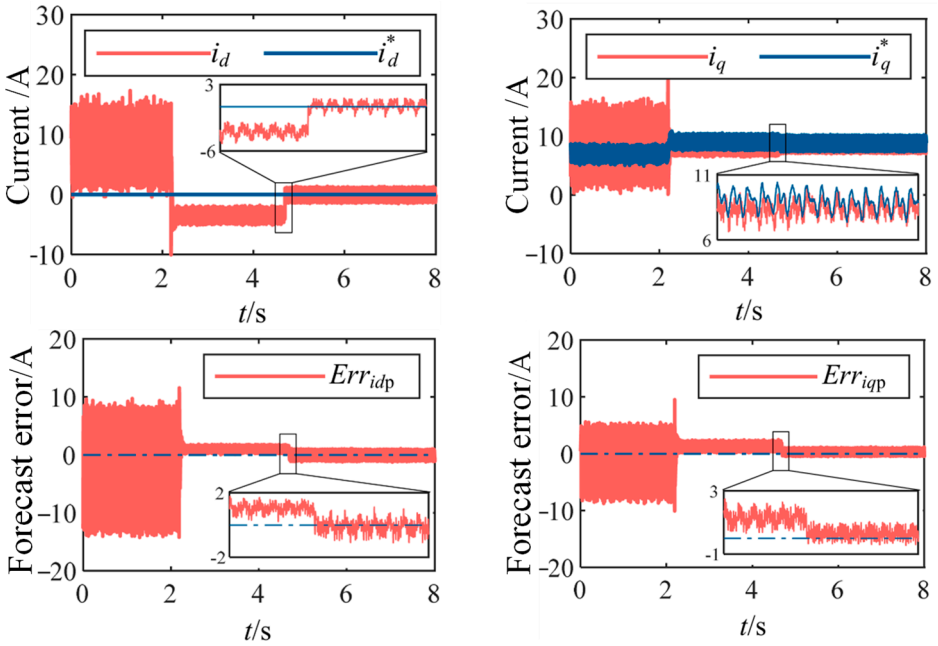


Figure 13. Algorithms gradual comparison experiment.

The results indicate that with the conventional method, both the tracking performance and prediction error of the d and q axis currents are significant. After activating the multi-coordinate synchronization algorithm, the prediction error is greatly reduced, and the fluctuation of the d and q axis currents decreases significantly, approaching the reference values more closely, though steady-state error still exists. After enabling the improved stator voltage equation-based models, the prediction error is further reduced, tracking accuracy is improved, and almost no steady-state error remains.

To validate the control precision of the proposed method during dynamic acceleration and deceleration processes, start-stop experiments were conducted under low carrier ratio conditions. The speed, phase current, and d and q axis current waveforms during the process in which the machine is started under load, accelerated to the rated speed of 370 r/min, and then decelerated to zero speed, all under a control frequency of 2 kHz, are shown in Figure 14. The results demonstrate that under low carrier ratio conditions, the proposed method maintains complete decoupling of the d and q axis currents during both acceleration and deceleration, with accurate tracking of the reference values, indicating high control precision even during transient processes.

Additionally, to verify the system stability and control performance of the proposed method under load variations, a sudden load increase experiment was conducted under low carrier ratio conditions. When the machine was operating at the rated speed of 370 r/min with a control frequency of 2 kHz, a 150% load step was applied (from 47 N m to 119 N m). The comparative experimental results using the conventional and proposed methods are shown in Figure 15. The results show that with the conventional method, the tracking performance of the d and q axis currents is poor and unstable before and after the load change, indicating that operating conditions significantly affect algorithm performance, and the prediction error is large. In contrast, the improved method maintains nearly zero prediction error before, during, and after the load transient, while preserving high tracking accuracy of the d and q axis currents. This confirms that the proposed method maintains high prediction accuracy and good control performance during dynamic processes and under various operating conditions, with minimal influence from load variations.

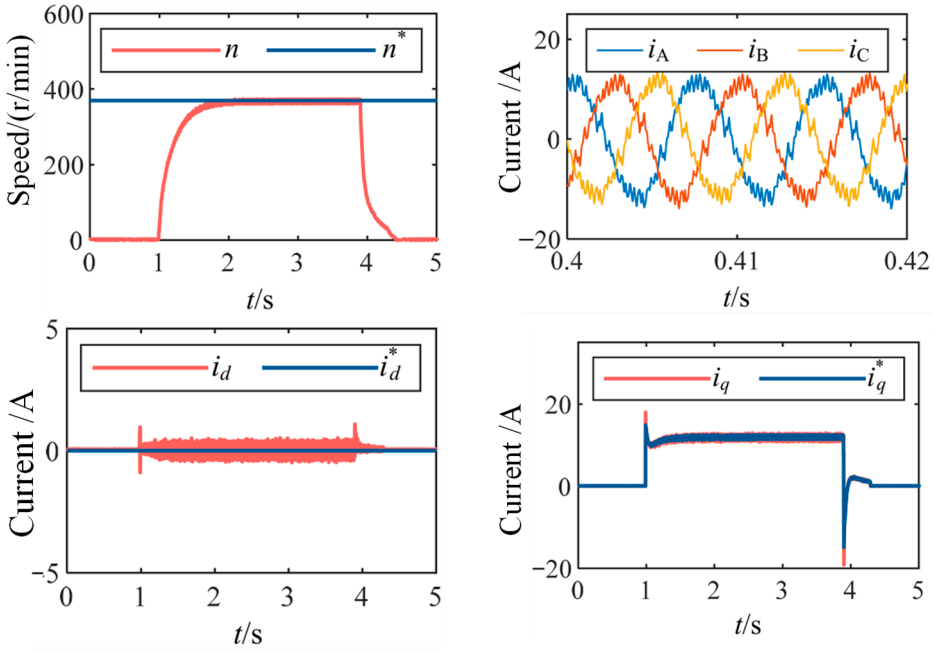
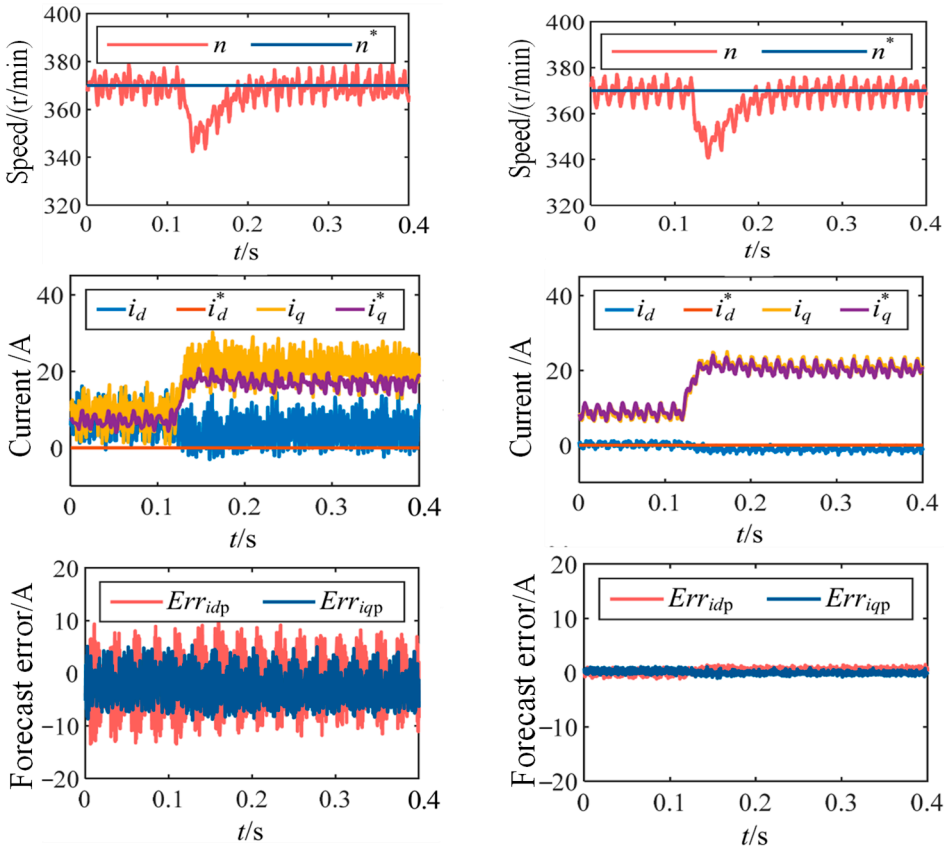


Figure 14. Start and stop experiments under low carrier ratio.



(**a**) Conventional method (**b**) Improved method

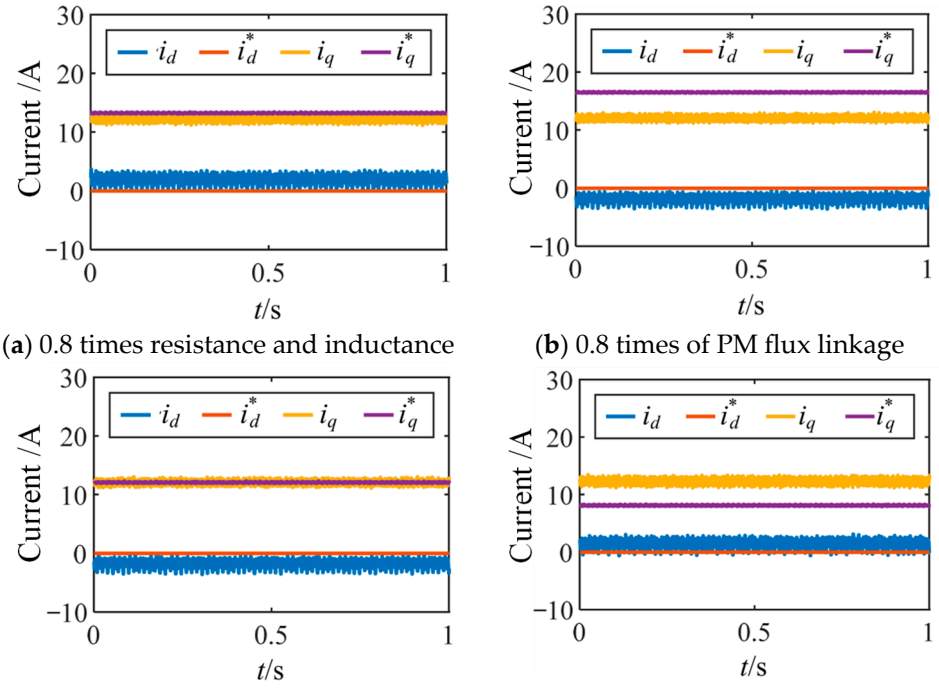
Figure 15. Step load experiments of both DPCC methods under low carrier ratio.

As demonstrated in the experimental results, the proposed method maintains stable operation and accurate tracking even at extremely low carrier ratios (down to 7.4), where both conventional DPCC and the reference methods exhibit significant performance degradation. Specifically, under CR = 7.4 conditions, our method achieves current THD below 8.2%, outperforming the adaptive method (THD > 12.5%) and the robust control

approach (THD > 15.3%). More importantly, the systematic addressing of multi-coordinate computational errors provides inherent advantages in dynamic response characteristics, as evidenced by the superior performance during start-stop transitions and load variations shown in Figures 14 and 15.

The comparative analysis confirms that the method not only resolves the specific limitations of conventional DPCC but also offers competitive advantages over other advanced predictive controllers, particularly in the challenging low carrier ratio regime that is critical for high-speed drive applications.

To verify the robustness of the proposed method against discrepancies between actual and nominal machine parameters, experiments were conducted under machine parameter mismatch conditions, including stator resistance and inductance mismatch, as well as rotor permanent magnet flux linkage mismatch. At the rated speed of 370 r/min and a control frequency of 2 kHz, the stator resistance and inductance parameters and the rotor permanent magnet flux linkage parameter in the controller were set to 0.8 and 1.2 times their calibrated values, respectively. The experimental results are shown in Figure 16. The results indicate that compared to variations in the rotor permanent magnet flux linkage, changes in the stator resistance and inductance parameters have a smaller impact on the performance of the proposed method.



(**a**) 0.8 times resistance and inductance (**b**) 0.8 times of PM flux linkage

(**c**) 1.2 times resistance and inductance (**d**) 1.2 times of PM flux linkage

Figure 16. Key machine parameters mismatch experiments.

6. Conclusions

In this paper, a permanent magnet synchronous machine (PMSM) model and a coordinate system synchronization method that accounts for rotor orientation errors are proposed for flywheel energy storage systems, achieving a precise deadbeat predictive current control (DPCC) strategy suitable for both high and low carrier ratio operations of PMSMs. Unlike incremental improvements to existing flux-oriented modeling approaches, the proposed method offers a fundamental reconceptualization of reference frame treatment in discrete control systems. The integration of a stationary *dq*-coordinate premise with systematic multi-coordinate synchronization addresses limitations that compensatory tech-

niques cannot overcome, particularly evident in the challenging low carrier ratio regime where conventional DPCC fails.

(1) By analyzing the sources of error in conventional deadbeat predictive current control under low carrier ratio conditions, a more accurate discrete-time PMSM model in the rotor reference coordinate is established. This model provides a precise representation of the intra-control-cycle behavior, thereby creating the foundation for further enhancing the accuracy of deadbeat control.

(2) Based on the improved machine model, a multi-coordinate system variable synchronization method is further proposed. This method eliminates computational errors caused by cross-coordinate spatial calculations, realizing a high-precision DPCC strategy applicable across a wide range of carrier ratios.

The results demonstrate that the proposed DPCC method exhibits superior torque-flux decoupling capability, along with improved prediction and tracking accuracy for *dq*-axis currents under low carrier ratio conditions. While the proposed method demonstrates improved performance, its effectiveness remains dependent on the accuracy of motor parameters. Future work will focus on integrating online parameter identification techniques to enhance robustness against parameter variations. Additionally, extending the control strategy to address operational scenarios under faulty conditions will be explored.

Author Contributions: Conceptualization, X.J. and Z.Z.; Methodology, X.J. and F.L.; Software, F.L.; Validation, F.L.; Formal analysis, Z.L. (Zhijian Ling); Resources, X.J.; Data curation, X.J. and Z.L. (Zhijian Ling); Writing—review & editing, H.Q. and Z.L. (Zhijian Ling); Visualization, H.Q., Z.Z. and Z.L. (Zhiru Li); Supervision, Z.Z.; Project administration, Z.L. (Zhiru Li); Funding acquisition, Z.L. (Zhiru Li). All authors have read and agreed to the published version of the manuscript.

Funding: This research was funded by the Key Research and Development of Zhenjiang grant number [GY2023011].

Data Availability Statement: The original contributions presented in this study are included in the article. Further inquiries can be directed to the corresponding author.

Conflicts of Interest: The authors declare no conflict of interest.

References

1. Yang, J.; Liu, P.; Ye, C.; Wang, L.; Zhang, X.; Huang, S. Multidisciplinary Design of High-Speed Solid Rotor Homopolar Inductor Machine for Flywheel Energy Storage System. *IEEE Trans. Transp. Electrif.* **2021**, *7*, 485–496. [CrossRef]
2. Huang, D.; Jiao, C.; Fang, J. Design and Research of a High-Temperature Superconducting Flywheel Energy Storage System with Zero-Flux Coils. *IEEE Trans. Appl. Supercond.* **2024**, *34*, 5702406. [CrossRef]
3. Chen, T.; Pei, Y.; Chai, F.; Shao, Y. Sideband Harmonic Model Considering Sampling Delay Effect in the PMSM Drives with Regular Sampled SVPWM Technique Under the Low Carrier Frequency Ratio. *IEEE Trans. Ind. Electron.* **2023**, *70*, 9914–9924. [CrossRef]
4. Wang, L.; Zhu, Z.Q.; Bin, H.; Gong, L. A Commutation Error Compensation Strategy for High-Speed Brushless DC Drive Based on Adaline Filter. *IEEE Trans. Ind. Electron.* **2021**, *68*, 3728–3738. [CrossRef]
5. Yan, Y.; Zhao, M.; Chen, Z.; Li, M.; Shi, T. Low frequency ratio deadbeat predictive torque control of permanent magnet synchronous motor in auxiliary coordinate system. *Proc. CSEE* **2023**, *43*, 761–769. (In Chinese)
6. Sun, J.; Wang, Z.; Gu, X.; Xia, C. Predictive current control of PMSM with high speed and low-frequency-ratio. *Proc. CSEE* **2020**, *40*, 3663–3672. (In Chinese)
7. Guo, J.; Fan, T.; Zhang, H.; Bian, Y.; Wen, X. Stability analysis of permanent magnet synchronous motor current loop control at high speed and low carrier ratio. *Proc. CSEE* **2019**, *39*, 7336–7346. (In Chinese)
8. Jarzebowicz, L. Errors of a Linear Current Approximation in High-Speed PMSM Drives. *IEEE Trans. Power Electron.* **2017**, *32*, 8254–8257. [CrossRef]
9. Bao, X.; Wang, X.; Peng, X. Review of key technologies of high-speed motor drive. *Proc. CSEE* **2022**, *42*, 6856–6870. (In Chinese)
10. Yepes, A.G.; Vidal, A.; Malvar, J.; López, O.; Doval-Gandoy, J. Tuning Method Aimed at Optimized Settling Time and Overshoot for Synchronous Proportional-Integral Current Control in Electric Machines. *IEEE Trans. Power Electron.* **2014**, *29*, 3041–3054. [CrossRef]

11. Zhang, Z.; Jing, L.; Zhao, Y.; Wu, X.; Yang, J.; Wang, J. Decoupling control of permanent magnet synchronous motor at high speed and low switching frequency. *Proc. CSEE* **2020**, *40*, 6345–6353. (In Chinese)
12. Bae, B.-H.; Sul, S.-K. A compensation method for time delay of full-digital synchronous frame current regulator of PWM AC drives. *IEEE Trans. Ind. Appl.* **2003**, *39*, 802–810. [CrossRef]
13. Dai, S.; Wang, J.; Sun, Z.; Chong, E. Deadbeat Predictive Current Control for High-Speed Permanent Magnet Synchronous Machine Drives with Low Switching-to-Fundamental Frequency Ratios. *IEEE Trans. Ind. Electron.* **2022**, *69*, 4510–4521. [CrossRef]
14. Yim, J.-S.; Sul, S.-K.; Bae, B.-H.; Patel, N.R.; Hiti, S. Modified Current Control Schemes for High-Performance Permanent-Magnet AC Drives with Low Sampling to Operating Frequency Ratio. *IEEE Trans. Ind. Appl.* **2009**, *45*, 763–771. [CrossRef]
15. Zhu, S.; Huang, W.; Yan, Y.; Niu, Z. High-Damped Complex Vector Current Regulator for PMSM Based on Active Damping Function. *IEEE Trans. Power Electron.* **2023**, *38*, 5204–5216. [CrossRef]
16. Wu, X.; Yuan, Q.; Fu, X.; Dai, P. A novel complex state current controller for synchronous motor at very low switching frequency. *Proc. CSEE* **2012**, *32*, 124–129. (In Chinese)
17. Song, Z.; Yao, W.; Li, W. Modeling of interior PMSM based on normal canonical form under low carrier ratio. *Proc. CSEE* **2023**, *43*, 4779–4789. (In Chinese)
18. Zhao, L.; Song, W.; Ruan, Z. Discrete Domain Design Scheme of Complex-Vector Current Controller for Induction Motor at Low Switching Frequency. *IEEE Trans. Transp. Electrif.* **2023**, *9*, 404–415. [CrossRef]
19. He, Y.; Wang, Z.; Zheng, S. Decoupling control of high speed permanent magnet synchronous motor based on online least squares support vector machine inverse system method. *Proc. CSEE* **2016**, *36*, 5639–5646. (In Chinese)
20. Xu, Y.; Li, S.; Zou, J. Integral Sliding Mode Control Based Deadbeat Predictive Current Control for PMSM Drives with Disturbance Rejection. *IEEE Trans. Power Electron.* **2022**, *37*, 2845–2856. [CrossRef]
21. Wang, Z.; Dai, B.; Guo, Z.; Yang, J. Single-Loop Current-Constrained Speed Regulation for PMSM via a Switching Controller. *IEEE Trans. Transp. Electrif.* **2025**, *11*, 5974–5982. [CrossRef]
22. Dai, B.; Wang, Z.; Zhao, J.; Li, S. Critical Current-Constrained Continuous Nonsingular Terminal Sliding Mode Control for PMSM Based on Control Barrier Function. *IEEE Trans. Power Electron.* **2025**, *40*, 15093–15103. [CrossRef]
23. Liu, Z.; Huang, X.; Hu, Q.; Li, Z.; Jiang, Z.; Yu, Y.; Chen, Z. A Modified Deadbeat Predictive Current Control for Improving Dynamic Performance of PMSM. *IEEE Trans. Power Electron.* **2022**, *37*, 14173–14185. [CrossRef]
24. Ji, J.; Qian, Y.; Zhao, W.; Tao, T.; Lu, H.; Wang, H. Variable switching sequence modulation strategy with low current ripple for dual three-phase PMSM operating at low switching-to-fundamental ratio. *Proc. CSEE* **2024**, *44*, 9422–9431. (In Chinese)

Disclaimer/Publisher's Note: The statements, opinions and data contained in all publications are solely those of the individual author(s) and contributor(s) and not of MDPI and/or the editor(s). MDPI and/or the editor(s) disclaim responsibility for any injury to people or property resulting from any ideas, methods, instructions or products referred to in the content.